MINISTRY OF EDUCATION AND TRAINING HO CHI MINH CITY UNIVERSITY OF TECHNOLOGY AND EDUCATION

TRAN THANH LAM

RESEARCH ON THE EFFECTS OF UNBALANCE PARAMETERS ON THE FATIGUE STRENGTH OF THE ROTOR

PH.D THESIS SUMMARY

MAJOR: MECHANICAL ENGINEERING

CODE: 9520103

Ho Chi Minh City, May 2025

ABSTRACT

In rotating powertrains such as engines, gearboxes or turbines; Especially for the power transmission shaft, dynamic unbalance often occurs due to fabrication errors, due to the asymmetrical design itself, due to the eccentric assembly process, uneven wear, or irrational mass distribution. Unbalances cause circulatory vibrations, creating stresses that vary over time – one of the main mechanisms that lead to fatigue damage. Many studies have focused on simulating and analyzing shaft fatigue under the influence of static and dynamic loads, but the separate effects of unbalance on fatigue strength still need to be clarified. Therefore, the study of parameters that cause unbalance including unbalanced mass, rotational velocity, etc. affecting the fatigue strength of the spindle is an urgent issue to ensure the reliability and working life of the drive system; specifically for the spindle. Some of the highlights that the thesis contributes to the field of study are stated below:

- Identify the technical parameters that directly affect the dynamic unbalance in the axis of rotation: rotation speed, eccentric mass and position of the unbalance mass.
- The vibration becomes unstable when the rotation speed reaches the critical speed and the displacement amplitude increases significantly. At the same time, the amount of unbalance increases (to G40) resulting in an increase in the displacement amplitude. The amplitude of the fluctuation in the case of G41.3 has $X = \pm 0.109$; $Y = \pm 0.135$ is even greater than the amplitude of fluctuation at critical speed 1: $X = \pm 0.101$; $Y = \pm 0.119$. This is the amplitude of fluctuation to be avoided during operation to ensure stable and long-term operation of the rotor.
- The initial phase angle of the test mass position, if a change occurs during operation, will result in different variations of the vibration phase causing the bending stress to increase or decrease which may result in failure appearing on the spindle.
- The results of this study also prove that the Newmark- β method is used to analyze the behavior of the rotor system with high reliability, unconditional stability, fast convergence time and high accuracy; with an error compared to the experiment < 6%.
- A new fatigue testing machine for studying the fatigue strength of unbalanced drive shafts has been developed. A new driver alignment tool is also designed to assess these unbalance effects.
- The results of the fatigue strength test showed that the fatigue limit and fatigue strength of the sample decreased under the influence of unbalanced factors; including test volume, operating speed and test load radius; compared to pure bending spindle; thereby constructing the fatigue curve of the C45 steel spindle under the effect of the impact force due to unbalance.
- In addition, the amplitude of oscillation gets larger and larger as the load cycle increases. This can be explained by the appearance and propagation of microcracks, amplifying the effect of unbalanced forces on the axis.

CHAPTER 1. GENERAL INTRODUCTION

1. Ask a question

Oscillation is a common phenomenon in nature and engineering, especially affecting building structures and industrial equipment. In particular, rotary equipment – a key mechanical mechanism – often generates vibrations, reducing system performance, causing product deviations and potentially technical problems. The main cause of vibration is unbalance, in addition to factors such as misalignment, material inhomogeneity, abrasion and impact. Vibration control in rotary equipment is a key factor in ensuring the stability and operational reliability of the system. The ISO 1940/1 - 2013 standard [1] has set permissible limits on the level of residual unbalance of the rotor, which plays an important role in the evaluation and control of vibration in rotating systems.

Rotor dynamics is a key area in the study of camera systems, which is essential for modern industry. Rotor vibration analysis focuses on key parameters such as rotational speed (especially critical speed), system stability, and dynamic response in the event of an unbalance [2,3].

Spindle destruction is one of the most common forms of damage in rotating mechanisms, with about 90% of cases stemming from fatigue cracking. Spindle fatigue strength is a key parameter in evaluating the service life and reliability of a mechanical system. The fatigue process originates from microcracks caused by cyclic oscillating stresses, which usually appear in large load-bearing areas on the surface of the part and develop over time, leading to complete failure [4].

Therefore, the analysis and evaluation of parameters affecting the dynamics of the rotor is of great significance to the fatigue durability that forms the basis for estimating the life of the part, contributing to the optimal planning of production and maintenance strategies. On the basis of that orientation, the project " *Research on the effects of unbalance parameters on the fatigue strength of the rotor*" has been proposed with the goal of investigating the parameters of the influence of the unbalance such as speed, position, initial phase angle, residual unbalance, and excitation impulse that will affect the fatigue endurance of the rotor in practice.

2. Research Objectives

2.1 General objectives

The calculation study evaluates the parameters that effect the unbalance on fatigue strength on the rotor by calculation and experiment.

2.2 Specific goals

Starting from the overall goal, the study proposes specific goals as follows to achieve the set orientation:

- Overview of the types of rotary mechanisms.
- Research and analysis of the characteristics of various types of rotating mechanisms, especially those that operate at high speeds, which are commonly used in industrial systems.
- Build a mathematical model for the research object.
- Matlab simulation calculation of the influence parameters.
- Design and manufacture machine models to serve the actual experiment process.
- Perform an experimental evaluation to analyze the impact of key parameters on the performance characteristics of the rotor.
- Determine the law of influence of some key parameters on fatigue durability on the rotor, create a scientific basis for evaluating the influence of these parameters on the service life (working time) so that the appropriate operating mode for the highest productivity can be determined.

3. Scope of study

Within the time and scope of the project, the research will focus on the following main contents:

- Material: C45 steel.
- The rotation speed ≤ 3000 rpm.
- The research content focuses on the parameters affecting unbalance on the rotor that are commonly used by domestic and foreign balancing units.
- The equipment is designed and manufactured for experiments such as oscillation surveyors and fatigue resistance surveyors.

4. Research Approach and Methods

4.1 Object of study

- Spindles and types of rotating parts
- High-speed mechanisms and cameras, both domestic and international, that are relevant to the research content will be consulted and analyzed.

4.2 Research Methodology

In order to achieve the set research objectives, the author implements the following methods:

- First, collect and study academic documents related to the phenomenon of fatigue in the rotating structure, in order to analyze the published works, thereby identifying the clarified contents and identifying unresolved problems — this will be the basis for the research. Along with that, a survey of the physical conditions and available equipment systems is carried out to select a deployment plan that is compatible with the limitations and capabilities of the project.

- Next, apply available equipment to process test samples in accordance with actual conditions; At the same time, it combines testing of physical and mechanical properties and evaluation of microstructure of metal materials.
- Then, the mathematical model is built and compared with the experimental results, followed by experiments and combined with the processing of the obtained experimental data to establish a fatigue curve equation that reflects the influence of parameters related to unbalance. Thereby, determining the applicable stress and the appropriate number of cycles for each specific working condition.

5 Scientific and practical significance

5.1 Scientific Significance

- Recommend the parameters to be surveyed to evaluate the rotor dynamics.
- To study the effects of factors including rotation speed n (vg/ph), position and initial phase angle of the test mass causing unbalance, along with the amount of residual unbalance, excitation impulse to stress that changes the dynamic behavior of the system.
- It proposes a method to calculate the change of stress, thereby helping to determine the relationship between fatigue destructive stress and characteristic parameters.
- Through the experimental results, the relationship between dynamic parameters and fatigue endurance was established.

5.2 Practical implications

- Determine the relationship between dynamic response and fatigue endurance on the rotor.
- Playing a fundamental role in developing production plans as well as maintenance strategies for equipment and machinery for domestic and foreign units.

6 Presentation structure of the thesis

The thesis consists of 6 chapters, illustrated by 52 drawings and 21 data tables. The content is organized according to the following layout:

Chapter 1. GENERAL INTRODUCTION

The content of this chapter introduces the urgency of the field related to the topic. From the analysis of the existing shortcomings, thereby setting out the research objectives of the focus of the topic and proposing the structure of the thesis.

Chapter 2. OVERVIEW

The content of this chapter presents the research situation in the fields related to the topic. The concepts of vibration, fatigue and destruction are covered. From the analysis of the existing gaps, thereby setting out the research orientation.

Chapter 3. MODELING THE DYNAMICS OF THE ROTOR SYSTEM

The content of this chapter builds mathematical models for research objects includes: from proposing and building models; design parameters; calculation method; calculation results, calculation dimensions and final results.

Chapter 4. ASSESSMENT RESULTS RANGE FROM CALCULATIONS AND EXPERIMENTS

A proposed displacement measuring device is designed and fabricated. The evaluation factors affecting the amount of unbalance on the rotor in the thesis used in simulation and experimental research are introduced in this chapter.

Chapter 5. RESULTS OF CALCULATION AND EXPERIMENT TO EVALUATE FATIGUE RESISTANCE A new device for measuring the fatigue strength of the rotor when it is out of balance is proposed to be designed and built. The results of the fatigue strength test showed that the fatigue limit and fatigue strength of the sample decreased under the influence of unbalanced factors; including test volume, operating speed and load radius.

Chapter 6. CONCLUSION AND DEVELOPMENT DIRECTION

This chapter presents a summary of the main research results achieved within the framework of the thesis. At the same time, a number of further research directions are also proposed to expand and develop the problems that have been studied. In addition, scientific publications related to the content of the thesis, including articles published in journals and specialized conferences, are listed to demonstrate the scientific nature and contribution of the thesis.

Chapter 2. OVERVIEW

1. The concept of an unbalance state on a rotor

Rotor unbalance occurs when the mass is unevenly distributed around the spindle, mainly due to fabrication errors, incorrect assembly, material inhomogeneity, geometric deformation, or wear during operation. Unbalance assessment is often based on factors such as eccentricity, tolerance error, material structure, impact, and tightness of the fitting.

2. Fatigue destruction mechanism in machine parts

Fatigue is noted as one of the common causes leading to the destruction of components with considerable frequency; in the breakdowns of industrial mechanical systems, directly affecting operational safety, production

efficiency and even human health. Because of that severity, the fatigue process has been the subject of intensive research for more than a century. The early contributions of scholars such as Schutz, Toth and Yarema laid the foundations for the perception of exhaustion destruction from the early days of the industrial revolution.

→ Within the limits of the research topic, we only consider the effect of stress on the fatigue strength of the exhaustion.

3. Overview of the research situation

An overview of the studies and the development of unbalance to fatigue endurance is presented in detail in the thesis, from the documents [14-78]. In the current period, fatigue strength analysis plays an essential role in evaluating the sustainable working ability of mechanical parts.

4. Research gaps and orientations

The results of the literature survey show that there is still no work that focuses on analyzing the impact of unbalance factors on the fatigue resistance of the rotating mechanism. Because in fact, the rotors before operation are balanced and during operation there is a maintenance plan (in terms of balance); in addition, some important/essential rotating mechanisms need to be equipped with Online Condition Monitoring (OCM) equipment. The requirement at this time is that the study will focus on analyzing the impact of unbalance factors on the fatigue resistance of the rotating mechanism, which cannot be balanced during operation or when the operation is unbalanced due to structural redistribution, material uniformity... Typical examples are the drive shafts in gearboxes, speed boxes, etc.

Chapter 3. MODELING THE DYNAMICS OF THE ROTOR SYSTEM

1. Building a mathematical model

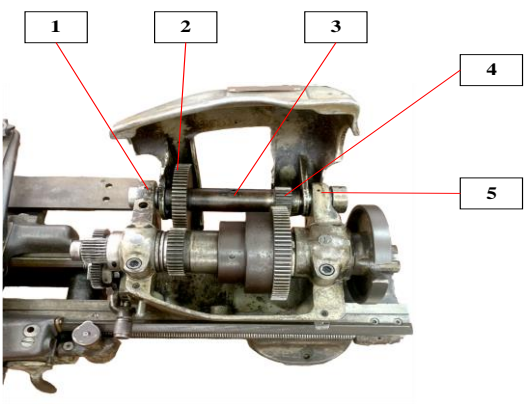


Figure 3.1 Shaft assembly – gear in the speed box

In this study, the cylindrical sample shown in Figure 2.3.c – corresponding to the four-point bending fatigue test method – was selected. This type of sample has the advantage of identifying and analyzing locations with a high risk of damage. It is proposed that the shaft assembly - gears with 2 gears mounted on the shaft as shown in Figure 2.1 have the ideal model as shown in Figure 2.4.

According to the ISO 1143 - 2010 standard for the model shaft in Figure 3.3 and the combination of the model in Figure 3.4, we propose a shaft – gear assembly for fatigue strength study as shown in Figure 3.2

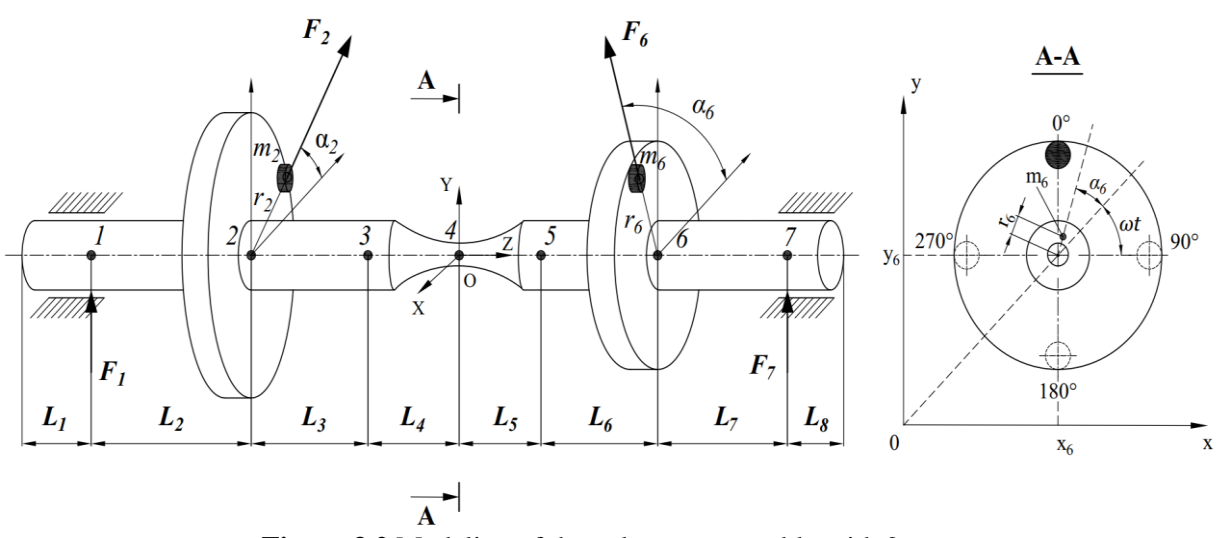


Figure 3.2 Modeling of the axle-gear assembly with 2 gears

From the above design, it is proposed to survey 7 important points on the spindle: points 1, 2, 3, 4, 5, 6, 7. In which, points 1 and 7 are the position of the pillow, points 2 and 6 are the position of the plate; points 3 and 5 are the positions with the largest cross-section on the axis; point 4 is the position with the smallest cross-section \rightarrow survey the fatigue strength of the shaft. Solve the above problem:

We have the x, y, torsion displacement α in this case:

$$q_i = [x_i, y_i, \alpha_i]^T \tag{3.1}$$

In which, the transposition in the x and y directions at the survey locations is:

which, the transposition in the x and y directions at the survey locations is:
$$x_i = [x_1, x_2, x_3, x_4, x_5, x_6, x_7]^T \qquad y_i = [y_1, y_2, y_3, y_4, y_5, y_6, y_7]^T$$

$$\alpha_i = [\alpha_1, \alpha_2, \alpha_3, \alpha_4, \alpha_5, \alpha_6, \alpha_7]^T \qquad \text{With } i = 1 \div 7;$$
 and
$$\begin{cases} x_i = x_n \text{ or } x_i = x_m + e_m cos \varphi_m \\ y_i = y_n \text{ or } y_i = y_m + e_m cos \varphi_m \end{cases}, \quad n = 1, 3, 5, 7; \quad m = 2, 4, 6$$
 Regarding the rotation angle, we focus on surveying the axis between 2 discs: from point 2 to point 6; Here;

Viewing the twist angle at the position of button 3 and button 5 is extremely small: $\alpha = 3 = 0$; The remaining 3 positions that need to be surveyed at this time are point 2, point 4 and point 6.

$$\alpha_j = \begin{bmatrix} \alpha_2 \\ \alpha_4 \\ \alpha_6 \end{bmatrix}$$
 With j = 2, 4, 6.
The equation for determining the angle of rotation is:

$$\boldsymbol{\varphi}_i = \boldsymbol{\alpha}_i + \boldsymbol{\omega}_i \boldsymbol{t} + \boldsymbol{\emptyset}_{\mathbf{0}_i} \tag{3.2}$$

At this time, I have a transposition:

$$\mathbf{x}_{i} = \begin{bmatrix} x_{1} \\ x_{2} + e_{2} \cos \varphi_{2} \\ x_{3} \\ x_{4} + e_{4} \cos \varphi_{4} \\ x_{5} \\ x_{6} + e_{6} \cos \varphi_{6} \\ x_{7} \end{bmatrix} \mathbf{y}_{i} = \begin{bmatrix} y_{1} \\ y_{2} + e_{2} \sin \varphi_{2} \\ y_{3} \\ y_{4} + e_{4} \sin \varphi_{4} \\ y_{5} \\ y_{6} + e_{6} \sin \varphi_{6} \end{bmatrix};$$

Velocity:

$$\dot{x}_{i} = \begin{bmatrix} \dot{x}_{1} \\ \dot{x}_{2} - e_{2}\dot{\varphi}_{2}\sin\varphi_{2} \\ \dot{x}_{3} \\ \dot{x}_{4} - e_{4}\dot{\varphi}_{4}\sin\varphi_{4} \\ \dot{x}_{5} \\ \dot{x}_{6} - e_{6}\dot{\varphi}_{6}\sin\varphi_{6} \\ \dot{x}_{7} \end{bmatrix} ; \qquad \dot{y}_{i} = \begin{bmatrix} \dot{y}_{1} \\ \dot{y}_{2} + e_{2}\dot{\varphi}_{2}\cos\varphi_{2} \\ \dot{y}_{3} \\ \dot{y}_{4} + e_{4}\dot{\varphi}_{4}\cos\varphi_{4} \\ \dot{y}_{5} \\ \dot{y}_{6} + e_{6}\dot{\varphi}_{6}\cos\varphi_{6} \end{bmatrix}$$

Angular Velocity:

$$\dot{\boldsymbol{\varphi}}_{\boldsymbol{j}} = \begin{bmatrix} \omega_2 + \dot{\alpha}_2 \\ \omega_4 + \dot{\alpha}_4 \\ \omega_6 + \dot{\alpha}_6 \end{bmatrix}$$

Kinetic energy of the system at this time:

$$T = T_t + T_t$$

At that time:

$$T = \frac{1}{2} [\dot{x}]^T [M_c] [\dot{x}] + \frac{1}{2} [\dot{y}]^T [M_c] [\dot{y}] + \frac{1}{2} [\dot{\phi}]^T [J_c] [\dot{\phi}]$$
(3.3)

With:

$$[M_c] = \begin{bmatrix} m_1 & 0 & 0 & 0 & 0 & 0 & 0 \\ 0 & m_2 & 0 & 0 & 0 & 0 & 0 \\ 0 & 0 & m_3 & 0 & 0 & 0 & 0 \\ 0 & 0 & 0 & m_4 & 0 & 0 & 0 \\ 0 & 0 & 0 & 0 & m_5 & 0 & 0 \\ 0 & 0 & 0 & 0 & 0 & m_6 & 0 \\ 0 & 0 & 0 & 0 & 0 & 0 & m_7 \end{bmatrix}$$
$$[J_c] = \begin{bmatrix} J_2 + m_2 e_2^2 & 0 & 0 \\ 0 & J_4 & 0 \\ 0 & 0 & J_6 + m_6 e_6^2 \end{bmatrix}$$

Jc: Moment of static inertia for survey points 2, 4, 6:

$$J_2 = \frac{1}{2}m_2R_2^2$$

$$J_4 = \frac{1}{2}m_4R_4^2$$

$$J_6 = \frac{1}{2}m_6R_6^2$$

 $J_6 = \frac{1}{2}m_6R_6^2$ Elastic potential of the system:

Elastic potential of the system:
$$V_{c} = \frac{1}{2}[x]^{T}[K_{x}][x] + \frac{1}{2}[y]^{T}[K_{y}][y] + \frac{1}{2}[\alpha]^{T}[K_{t}][\alpha]$$

$$K_{x} = K_{y} = \begin{bmatrix} (k_{1} + k_{2}) & -k_{2} & 0 & 0 & 0 & 0 & 0 \\ 0 & (k_{2} + k_{3}) & -k_{3} & 0 & 0 & 0 & 0 \\ 0 & -k_{3} & (k_{3} + k_{4}) & -k_{4} & 0 & 0 & 0 \\ 0 & 0 & -k_{4} & (k_{4} + k_{5}) & -k_{5} & 0 & 0 \\ 0 & 0 & 0 & -k_{5} & (k_{5} + k_{6}) & -k_{6} & 0 \\ 0 & 0 & 0 & 0 & -k_{6} & (k_{6} + k_{7}) & 0 \\ 0 & 0 & 0 & 0 & 0 & 0 & 0 & 0 \end{bmatrix}$$
In which:

In which:

 $-k_2$, k_3 , k_4 , k_5 , k_6 : anti-bending hardness

$$-k_2, k_3, k_4, k_5, k_6$$
: anti-bending nardness $-k_1, k_7$: stiffness at the support position
$$k_2 = \frac{3EI}{l_2^3}; \; ; ; ; k_3 = \frac{12EI}{(l_2 + l_3)^3} k_4 = \frac{6EI}{l_4^3} k_5 = \frac{3EI}{l_5^3} \; k_6 = \frac{3EI}{l_6^3}$$

Since the spindle system is a spatially continuous system, numerical solutions are applied to discrete it into a multi-order system. This process allows the continuous system to be represented by a multi DOF system. From the above design, it is proposed to survey 7 characteristic points along the axis of rotation, including:

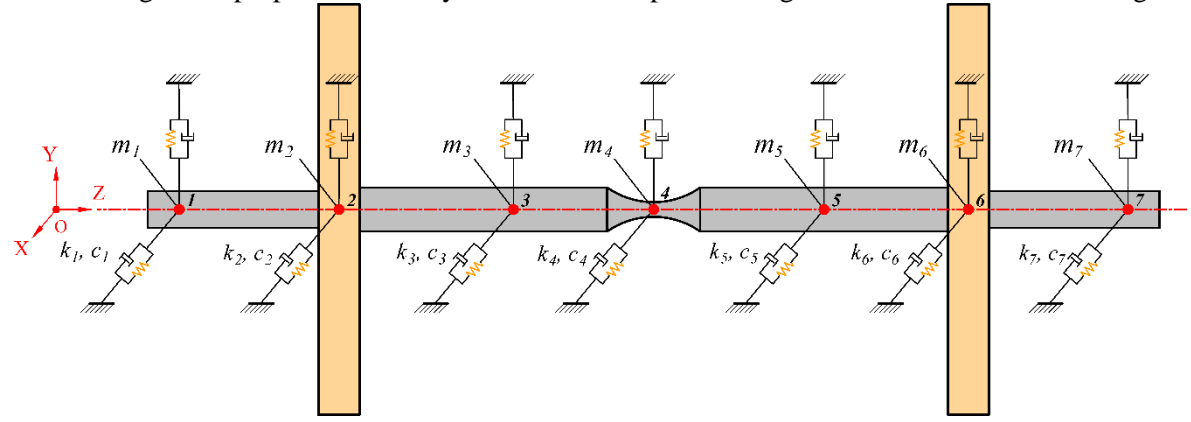


Figure 3.3 Physical model of the shaft and 2 discs

So; in this problem; The spindle is twisted (extremely small) due to the forces that appear at points 1 and 7 on the model.

Regarding the rotation angle, we focus on surveying the axis between the 2 discs: from point 2 to point 6. Here; The twist angle at button 3 and button 5 is extremely small: $\alpha 3 = \alpha 5 = 0$; the remaining 3 positions that need to be surveyed at this time are point 2, point 4 and point 6.

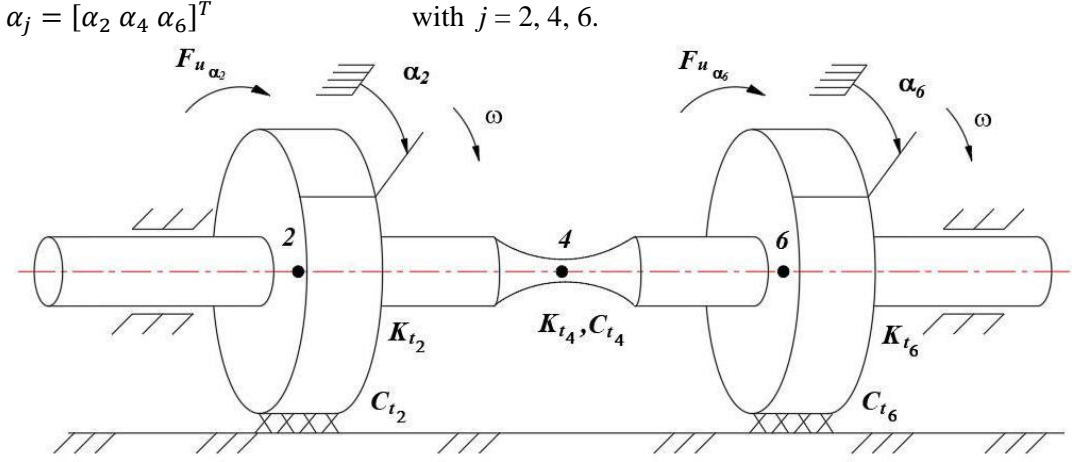


Figure 3.4 Modeling of the twisted survey shaft from points 2 to 6

Elastic potential energy of model 3.4:

$$V = \frac{1}{2}k_{t_2}\alpha_2^2 + \frac{1}{2}k_{t_4}(\alpha_2 - \alpha_4)^2 + \frac{1}{2}k_{t_6}(\alpha_4 - \alpha_6)^2$$
(3.5)

$$\begin{aligned} \frac{\partial V}{\partial \alpha_2} &= k_{t_2} \alpha_2 + k_{t_4} (\alpha_2 - \alpha_4) \\ \frac{\partial V}{\partial \alpha_4} &= -k_{t_4} (\alpha_2 - \alpha_4) + k_{t_6} (\alpha_4 - \alpha_6) \\ \frac{\partial V}{\partial \alpha_6} &= -k_{t_6} (\alpha_4 - \alpha_6) \end{aligned}$$

At this time, the anti-torsion hardness of the shaft:

$$\mathbf{K_T} = \begin{bmatrix} k_{t_2} + k_{t_4} & -k_{t_4} & 0 \\ -k_{t_4} & k_{t_4} + k_{t_6} & -k_{t_6} \\ 0 & -k_{t_6} & k_{t_6} \end{bmatrix}$$

$$k_{t_2} = \frac{GI_p}{l_2}$$
; $k_{t_4} = \frac{GI_p}{l_2 + l_3 + l_4}$; $k_{t_6} = \frac{GI_p}{l_5 + l_6}$

Dissipative energy of the system:

$$D = \frac{1}{2} [\dot{x}]^T [C_x] \{\dot{x}\} + \frac{1}{2} [\dot{y}]^T [C_y] \{\dot{y}\} + \frac{1}{2} [\dot{\alpha}]^T [C_t] \{\dot{\alpha}\}$$
(3.6)

Dissipative energy of the system:
$$D = \frac{1}{2} [\dot{x}]^T [C_x] \{\dot{x}\} + \frac{1}{2} [\dot{y}]^T [C_y] \{\dot{y}\} + \frac{1}{2} [\dot{\alpha}]^T [C_t] \{\dot{\alpha}\}$$

$$C_x = C_y = \begin{bmatrix} -(c_1 + c_2) & -c_2 & 0 & 0 & 0 & 0 & 0 \\ -c_2 & (c_2 + c_3) & -c_3 & 0 & 0 & 0 & 0 \\ 0 & -c_3 & (c_3 + c_4) & -c_4 & 0 & 0 & 0 \\ 0 & 0 & -c_4 & (c_4 + c_5) & -c_5 & 0 & 0 \\ 0 & 0 & 0 & -c_5 & (c_5 + c_6) & -c_6 & 0 \\ 0 & 0 & 0 & 0 & -c_6 & (c_6 + c_7) & 0 \\ 0 & 0 & 0 & 0 & 0 & 0 & 0 & 0 \end{bmatrix}$$
Time: We have the dissipative energy of the damper in Figure 3.6 as follows:

At this time; We have the dissipative energy of the damper in Figure 3.6 as follows:

$$D = \frac{1}{2}C_{t_2}\dot{\alpha}_2 + \frac{1}{2}C_{t_2}(\dot{\alpha}_2 - \dot{\alpha}_4)^2 + \frac{1}{2}C_{t_3}(\dot{\alpha}_4 - \dot{\alpha}_6)^2$$
At that time, the anti-torsion damping at this time:
(3.7)

$$C_T = \begin{bmatrix} C_{t_2} + C_{t_4} & -C_{t_4} & 0 \\ -C_{t_2} & C_{t_4} + C_{t_6} & -C_{t_6} \\ 0 & -C_{t_6} & C_{t_6} \end{bmatrix}$$

In which

 C_{t_2} ; C_{t_4} ; C_{t_6} are anti-torsional dampers at positions 2, 4, 6 as surveyed.

The Lagrange equation of the system at this time:

$$\frac{d}{dt} \left(\frac{\partial T}{\partial \{\dot{q}_i\}} \right) - \frac{\partial T}{\partial \{\dot{q}_i\}} + \frac{\partial D}{\partial \{\dot{q}_i\}} + \frac{\partial V}{\partial \{\dot{q}_i\}} = F_i$$
(3.8)

With Impact Force:

$$\overrightarrow{F_l} = \overrightarrow{F_{g_l}} + \overrightarrow{F_{u_l}} + \overrightarrow{F_{m_l}}$$

 $\overrightarrow{F_l} = \overrightarrow{F_{g_l}} + \overrightarrow{F_{u_l}} + \overrightarrow{F_{m_l}}$ Differential equation of rotor motion at this time:

$$[M]\{\ddot{q}\} + [C]\{\dot{q}\} + [K]\{q\} = \{F_{g_i}\} + \{F_{u_i}\} + \{F_{m_i}\}$$
(3.9)

In which:

+ : Mass matrix of the system $[M]_{17x17}$

+ : Damping Matrix[C]_{17x17}

+ : Hardness matrix $[K]_{17x17}$

+: The displacement vector consists of x, y and rotation angles. $\{q\}_{17x1}$

+ : External force vector $\{F_i\}_{17x1}$

$$\overrightarrow{F_l} = \overrightarrow{F_{g_l}} + \overrightarrow{F_{u_l}} + \overrightarrow{F_{m_l}}$$

In which:

- F_{g_i} : The force caused by the point mass weight.
- $\vec{F_{u_i}}$: Centrifugal force due to unbalance.
- F_{m_i} : External stimulus.

With:

Equation (3.10) rewrites:

$$\begin{split} F_{u_{x_2}} &= m_2 e_2 (\dot{\varphi}_2^2 \cos \varphi_2 + \ddot{\varphi}_2 \sin \varphi_2) \\ F_{u_{x_4}} &= m_4 e_4 (\dot{\varphi}_4^2 \cos \varphi_4 + \ddot{\varphi}_4 \sin \varphi_4) \\ F_{u_{x_6}} &= m_6 e_6 (\dot{\varphi}_6^2 \cos \varphi_6 + \ddot{\varphi}_6 \sin \varphi_6) \\ F_{u_{y_2}} &= m_2 e_2 (\dot{\varphi}_2^2 \sin \varphi_2 - \ddot{\varphi}_2 \cos \varphi_2) \\ F_{u_{y_4}} &= m_4 e_4 (\dot{\varphi}_4^2 \sin \varphi_4 - \ddot{\varphi}_4 \cos \varphi_4) \\ F_{u_{y_6}} &= m_6 e_6 (\dot{\varphi}_6^2 \sin \varphi_6 - \ddot{\varphi}_6 \cos \varphi_6) \\ F_{u_{\alpha_2}} &= m_2 e_2 (\ddot{x}_2 \sin \varphi_2 - \ddot{y}_2 \cos \varphi_2) \\ F_{u_{\alpha_4}} &= m_4 e_4 (\ddot{x}_4 \sin \varphi_4 - \ddot{y}_4 \cos \varphi_4) \\ F_{u_{\alpha_6}} &= m_6 e_6 (\ddot{x}_6 \sin \varphi_6 - \ddot{y}_6 \cos \varphi_6) \end{split}$$

2. Calculation method

Using the Beta-Newmark time-step analysis method to solve the equation (3.9) as follows:

$$[M]{\ddot{q}} + [C]{\dot{q}} + [K]{q} = {F_q} + {F_u} + {F_m}$$

Inform:

$$\{q_i\}, \{\dot{q}_i\}, [M], [C], [K], \{F_q\}, \{F_u\}, \{F_m\} \Delta t, t_i, \gamma, \beta$$

$$\ddot{q}_{i} = [M]^{-1} \left(-[C] \{ \dot{q}_{i} \} - [K] \{ q_{i} \} + \{ F_{g} \} + \{ F_{u} \} + \{ F_{m} \} \right)$$

$$\begin{cases} q_{i+1} = q_{i} + \Delta t \dot{q}_{i} + (0.5 - \beta) \Delta t^{2} \ddot{q}_{i} + \beta \ddot{q}_{i+1} \Delta t^{2} \\ \dot{q}_{i+1} = \dot{q}_{i} + (1 - \gamma) \Delta t \ddot{q}_{i} + \gamma \Delta t \ddot{q}_{i+1} \\ M \ddot{q}_{i+1} + C \dot{q}_{i+1} + K q_{i+1} = \mathbf{F}_{i+1} \end{cases}$$
(3.11)

Develop:

$$[M + C\gamma \Delta t + K\beta \Delta t^{2}]\ddot{q}_{i+1} = F_{i+1} - C[\dot{q}_{i} + (1 - \gamma)\Delta t \ddot{q}_{i}] - K[q_{i} + \Delta t \dot{q}_{i} + (0.5 - \beta)\Delta t^{2} \ddot{q}_{i}]$$
(3.13) Rewrite equation (3-20) to:

$$\widehat{K}\ddot{q}_{i+1} = \hat{f}_{i+1} \tag{3.14}$$

In which:

$$K = [M + C\gamma \Delta t + K\beta \Delta t^2]$$

$$|f_{i+1}| = F_{i+1} - C|[\dot{q}_i + (1-\gamma)\Delta t \ddot{q}_i] - K[q_i + \Delta t \dot{q}_i + (0.5-\beta)\Delta t^2 \ddot{q}_i]|$$

 $\hat{f}_{i+1} = F_{i+1} - C\big[[\dot{q}_i + (1-\gamma)\Delta t \ddot{q}_i] - K[q_i + \Delta t \dot{q}_i + (0.5-\beta)\Delta t^2 \ddot{q}_i]\big]$ With adjustable parameters during loop processing. Give: γ , β : $\gamma = \frac{1}{2}$; $\beta = \frac{1}{4}$; $\Delta t = 0.01$; unconditional stability [90, 91]. We have an algorithmic flowchart as shown in Figure 3.7

3. Calculation results

Results calculated by matlab: displacement, torsion angle with speed: 2000 rpm (ignoring the effect of damping) at point 4.

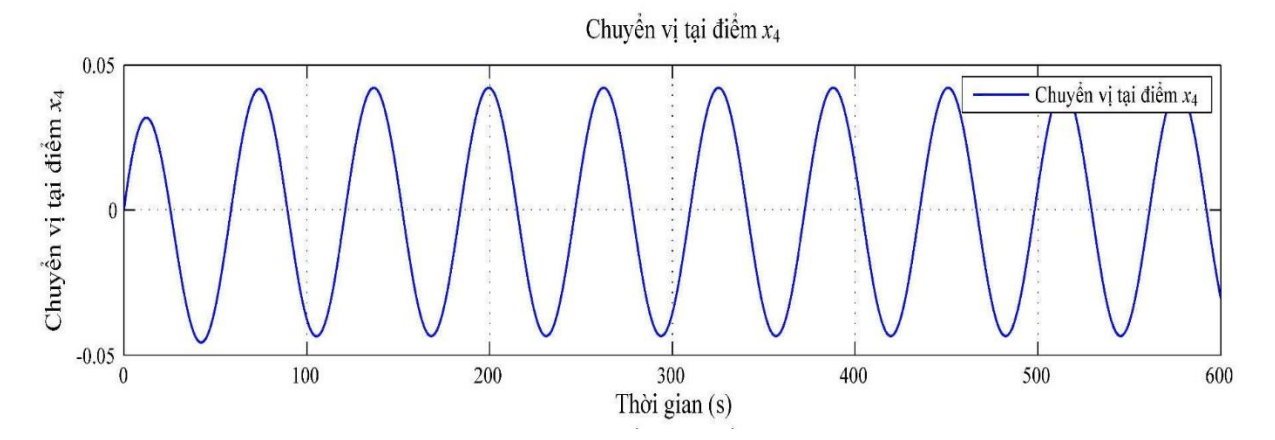


Figure 3.5 X-axis displacement at point 4

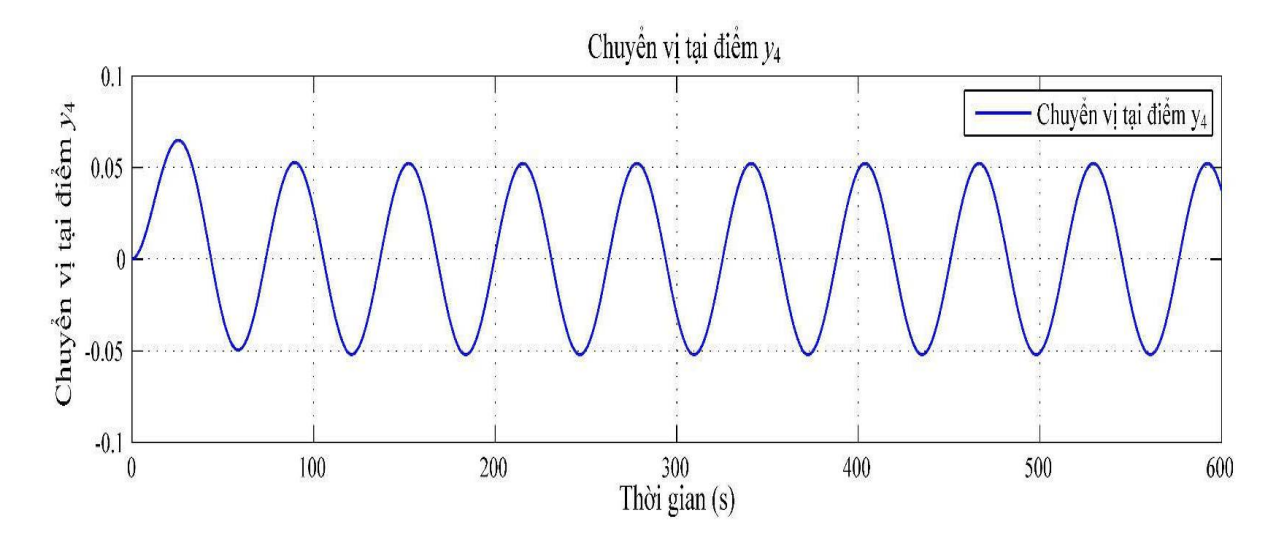


Figure 3.6 Y-axis displacement at point 4

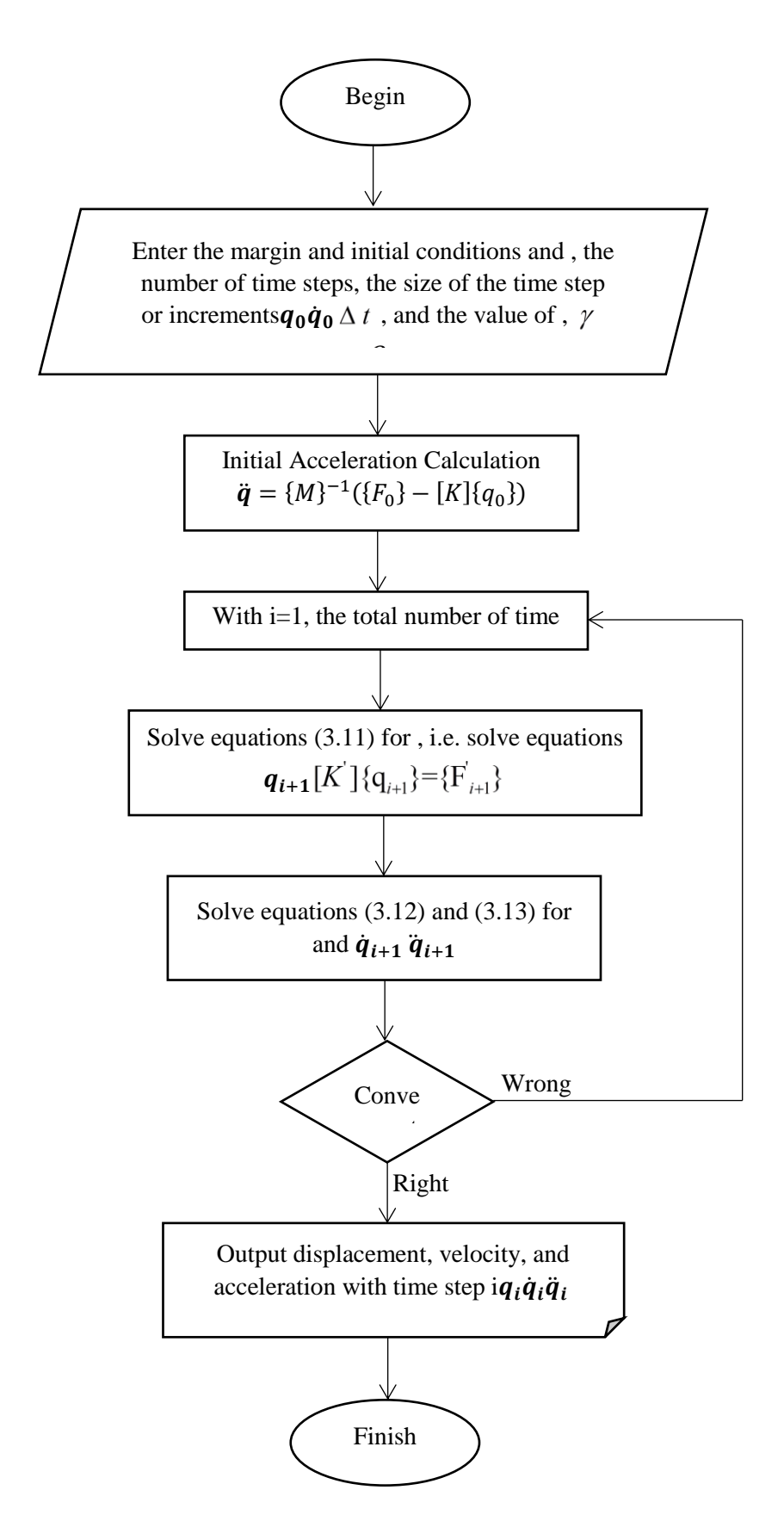


Figure 3.7 Algorithm flow chart of the mathematical model

 Table 3.1 Specifications of Survey Shafts and Discs

	Specifications	Value	Unit
L	Shaft Length	0.256	m
$l_1 = l_8$	"	0.008	m
$l_2 = l_7$	"	0.045	m
$l_3 = l_6$	"	0.040	m
$l_4 = l_5$	"	0.035	m
D_{shaft}	Shaft diameter	0.012	m
Disk	Disc Diameter	0.1	m
В	Disc thickness	0.02	m
F_2	Initial phase angle at point 2	0	line
F_6	Initial phase angle at point 6	0	line
e_2	Eccentricity	4.7*10-3	m
e 6	Eccentricity	4.7*10-3	m
K_r	Shaft stiffness	7*10 ⁷	N/m
K_b	Stiffness of the support pillow	$7.2*10^6$	N/m
K_t	Torsional stiffness of the shaft	0	N.m/rad
С	Cushion cushioning	20	Nm/s
μ	Friction coefficient	0.002	
υ	Poisson coefficient	0.28	
ρ	Specific gravity	7.8*103	kg/m ³
m_{shaft}	Shaft mass	0.285	medical history
m_{disk}	Disc mass	0.2	medical history
m	Shaft and rotor mass	0.685	medical history
$m_1 = m_7$	Button 1 and Button 7 Volumes	0.015	medical history
$m_2 = m_6$	Node 2 and Button 6 Volumes	0.035	medical history
$m_3 = m_5$	Volume of 3 and 5 nodes	0.08	medical history
m_4	Button Volume 4	0.025	medical history
g	Field Acceleration	9.81	m/s ²
I_p	Moment of inertia	1.2*10-7	m^4
E	Modun đàn hồi Young	2.1*1011	N/m ²
G	Twisted Module	$7.7*10^{10}$	N/m ²
Ct	Torsional damping of the shaft	0	Ns/rad
\mathcal{O}_n	Rotation speed	209	rad/s

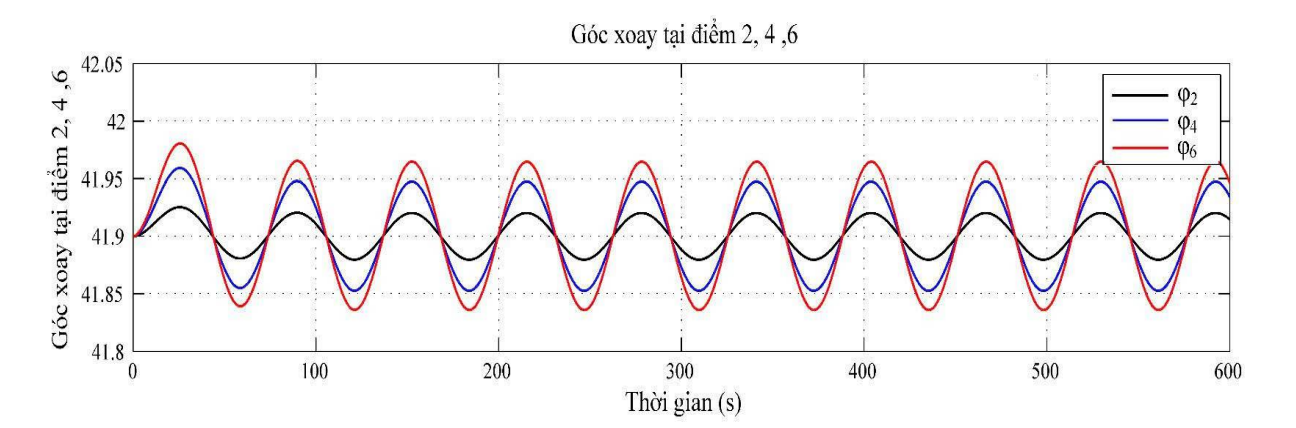


Figure 3.8 Rotation angle at point 2, point 4 and point 6

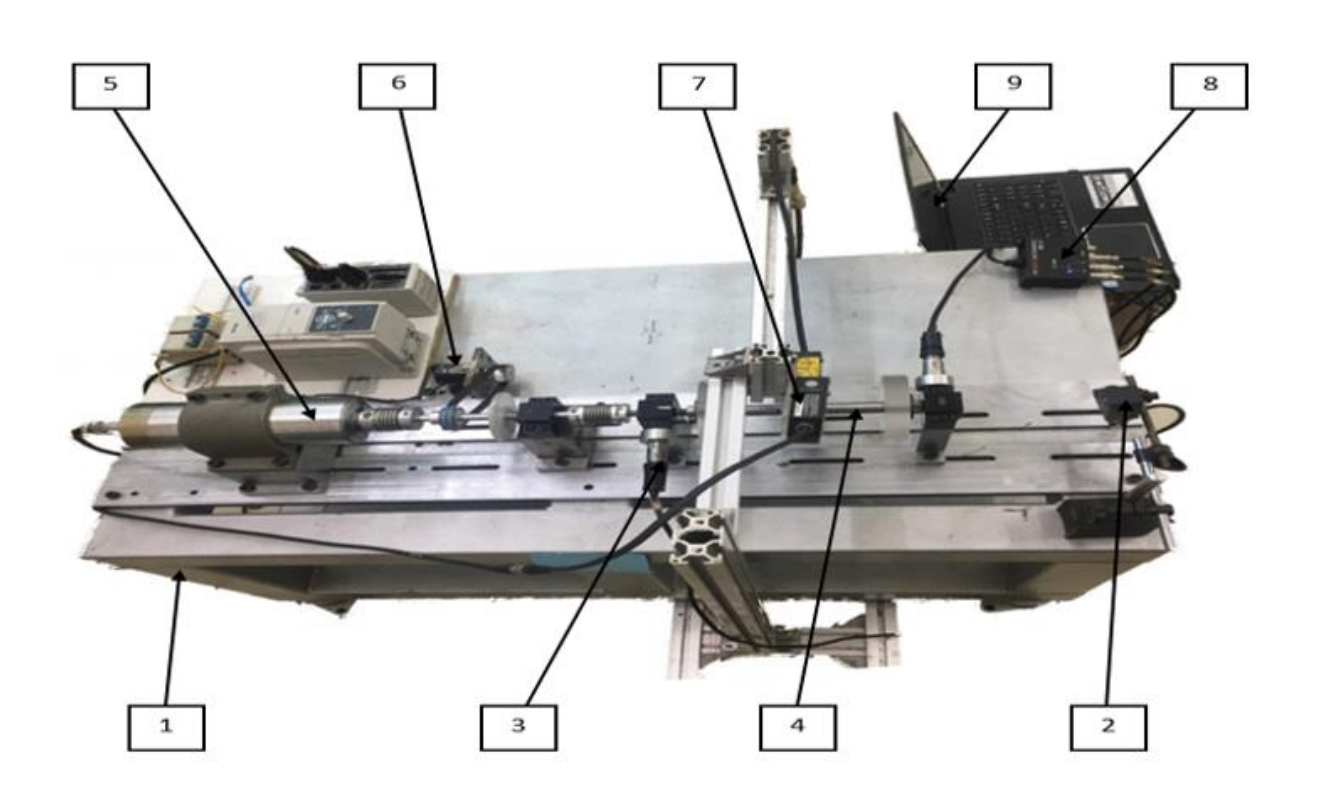
Table 3.2 Calculation of displacement and rotation angle at point 4

Location	Value	Transposition X (mm)	Transposition Y (mm)	Torsional angle (rad)	Notes
Doint 4	Min	-0,045	-0,053	0,059	
Point 4	Max	0,042	0,065	-0,048	

Assess:

Based on the results of the calculations obtained, it can be seen that the parameters are characteristic at point 4; including X-direction disposition, Y-direction displacement and rotation angle; clearly shown in Table 3.5. In particular, the rotation angle value at point 4 is very small, outside the measurement limit of existing experimental equipment. Therefore, within the scope of this study, the effect of the rotation angle at point 4 is considered negligible and negligible. The analysis and evaluation of kinetics at this point will focus on two linear displacement parameters in the X and Y directions to ensure the accuracy and practicality of the research model.

Chapter 4. ASSESSMENT RESULTS RANGE FROM CALCULATIONS AND EXPERIMENTS 4.1 Design and construction of oscillation meters



 $1.Base-2.\ Optical\ Sensor-3.\ Acceleration\ Sensor-4.Rotor-5.Motor-6.\ Encoder-7.\ Keyence\ Sensor-8.DAQ-9.Comp$

Figure 4.1 Oscillator Experimental Equipment

4.2 Influencing factors

4.2.1 Effect of rotation speed (Critical speed)

When the rotor operates close to the critical speed 1 (mode 1), its oscillation shape will correspond to the simulation shown in figure 4.5

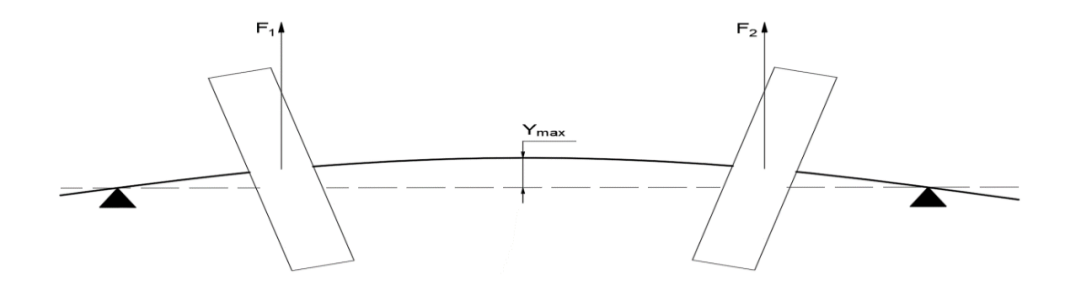


Figure 4.2 Rotor oscillation shape in critical mode 1

In the case of ignoring the effect of the damping factor c, the first-order critical speed can be determined according to the formula [2]:

$$\omega_{cr_1} = \sqrt{\frac{k}{m}} = \sqrt{\frac{E.A}{L.m}} = \sqrt{\frac{2,1.10^{11}.3,14.0.01^2}{4.0,256.0,680}} = 313 \, rad/s$$

Where: k: rotor hardness; m: rotor mass; L: shaft length; A: shaft cross section

At this time, the corresponding rotor rotation speed value is:

$$n_{cr_1} = \frac{60.\,\omega_1}{2\pi} = \frac{60.313}{2.3.14} = 3000 \,\text{vong/phút}$$

 $n_{cr_1} = \frac{60.\omega_1}{2\pi} = \frac{60.313}{2.3,14} = 3000 \ v \\ ong/ph \\ út$ In order to ensure that the rotor in the model operates stably and in accordance with the actual rotational speed ranges commonly encountered in mechanical equipment, the speed levels selected for the experiment include: n1 =800 rpm, $n^2 = 1500$ rpm and $n^3 = 2000$ rpm. Note that the speed $n^3 = 2000$ rpm is less than 70% of , i.e. it is still below the critical speed threshold [4, 5]. The results obtained from the experimental measurement process at these 3 speeds show that the rotor operates stably, which is clearly shown in Table 4.1 and figure 4.6.

Table 4.1 Results of displacement measurements along the X and Y axes at node 4

Frequenc	Speed	Newmark-b		Experi	Error		
y(Hz)	(rpm)	X (mm)	Y (mm)	X (mm)	Y (mm)	X	He
34	2000	± 0.043	± 0.071	± 0.046	± 0.081	6 %	12 %
51	3000	± 0.085	± 0.097	± 0.101	± 0.119	15 %	18 %

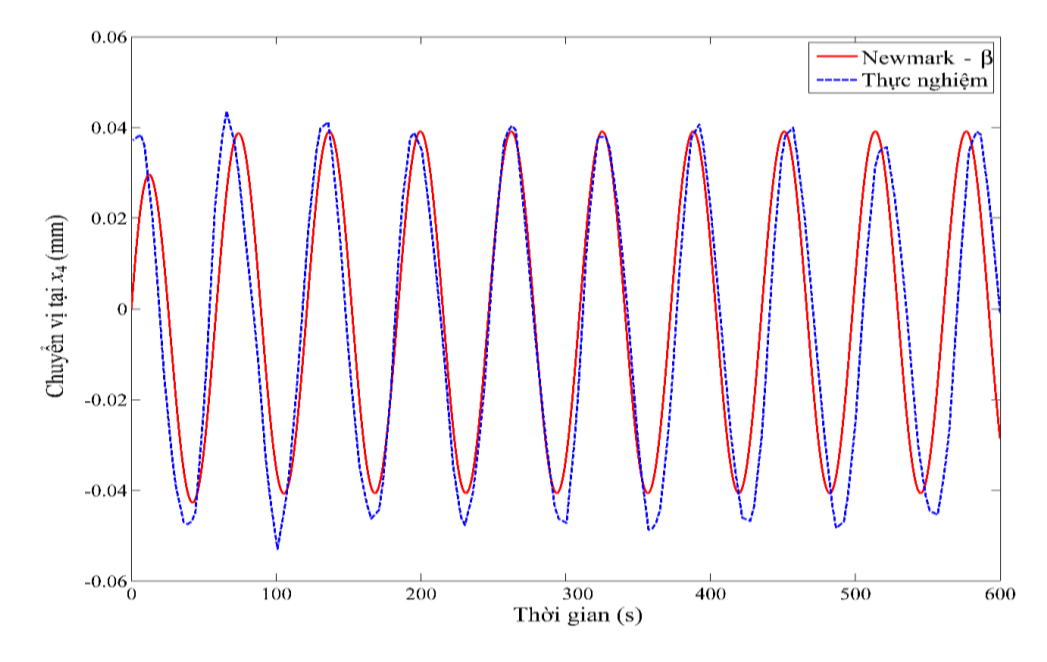


Figure 4.3 Displacement at node 4 in the X direction between the Newmark–β method and the experimental method at n = 2000 rpm

Observe:

From the calculation results (table 3.1) to the experimental results (table 4.1), it is shown that the calculation results and experimental results at X-axis displacement are reliable.

The relative error at X-axis displacement (n = 2000 rpm) is:

$$\varepsilon = \frac{0.046 - 0.043}{0.046} = 6\%$$

3.2.2 Effects of unbalance

Based on the ISO 1940/1 – 2013 standard on unbalance limits, the test volume of the mtrial and the allowable eccentricity e corresponding to the balance levels G1, G2.5, G6.3, G16 and G40 have been determined through calculation [1].

For G1, the emin allowable eccentricity $(n_3 = 2000 \text{ rpm})$ is:

4
$$e_{min} = \frac{G1}{\omega_3} = \frac{1}{209} = 4,7.10^{-3} \text{ mm}$$

For G1, the emin allowable eccentricity $(n_3 - 2000 \text{ ipm})$ is: $4 \qquad e_{min} = \frac{G1}{\omega_3} = \frac{1}{209} = 4,7.10^{-3} \text{ mm}$ Similarly; for the G40, the maximum allowable eccentricity emax (nI = 800 rpm) is: $5 \qquad e_{max} = \frac{G40}{\omega_1} = \frac{40}{84} = 0,47 \text{ mm}$

5
$$e_{max} = \frac{G40}{\omega_1} = \frac{40}{84} = 0,47 \text{ mm}$$

In which, for the G16 level, the *mtrial test volume* calculated at the lowest rotation speed of nl = 800 rpm is determined as follows:

6
$$m_{trial} = \frac{k.9,54.G_{16}.M_{rotor}}{n_1.r} = 26.1 g$$

 $6 \qquad m_{trial} = \frac{k.9,54.G_{16}.M_{rotor}}{n_1.r} = 26.1~g$ Therefore, the selected test weight values are 10g, 20g and 30g, respectively; applies to previously recommended rotation speed levels.

Case 1: Set the test volume to set the symmetry (position 00 - 00)

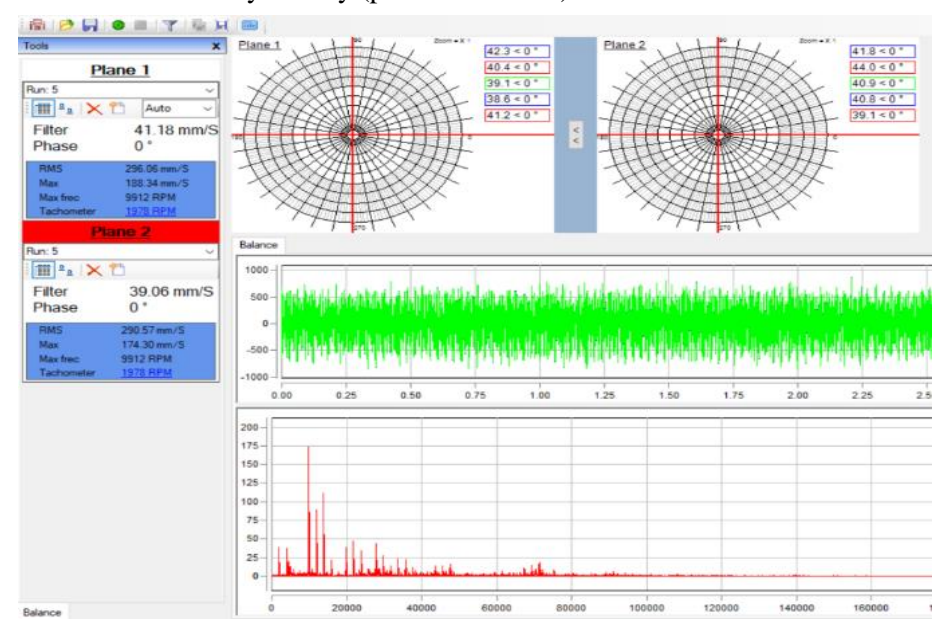


Figure 4.4 Measurement value of unbalance on 2 planes at position 00 - 00; mtrial = 30g.

The data on the amount of rotor unbalance at position 00 - 00, corresponding to each of the different load levels, are presented in Table 4.2

Table 4.2 Unbalance values recorded when testing at position 00 - 00

No	Trial Mass (grams)	Speed (rpm)	$G = e_p.\omega$ (mm/s)
1		800	0.58
2	0	1500	1.12
3		2000	1.34
4		800	0.9
5	10	1500	4.9
6		2000	20.5
7	20	800	1.1

No	Trial Mass (grams)	Speed (rpm)	$G = e_{p} \cdot \omega$ (mm/s)
8		1500	9.4
9		2000	32.8
10		800	2.2
11	30	1500	14.3
12		2000	41.1

Accordingly, we have the results of translocation measurements

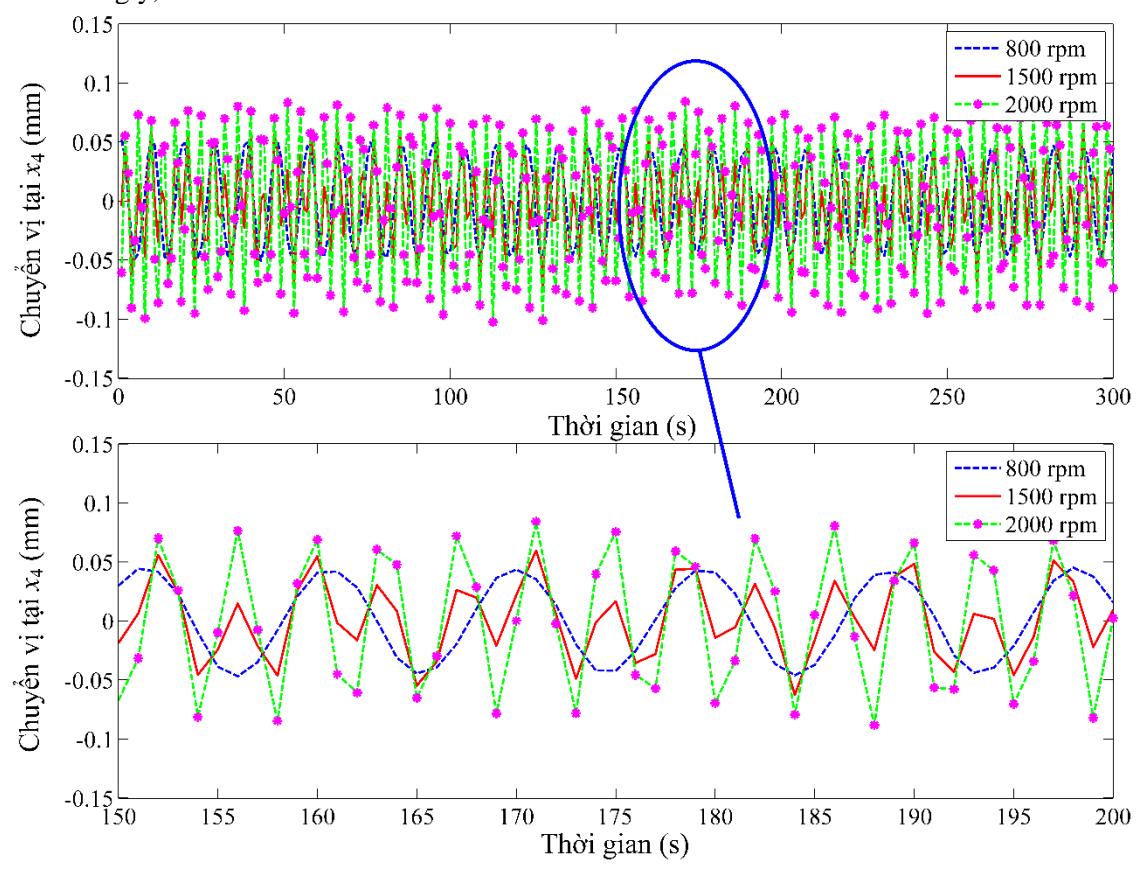


Figure 4.5 X-directional displacement of button 4 with mtrial = 20g at 800, 1500 and 2000 rpm

Evaluation: Figure 4.5 and Table 4.2 show the change of horizontal displacement (X-axis) at button 4 at different operating speeds. At rotation speed n3 = 2000 rpm, the oscillation of the rotor in the state of unbalance reaches its greatest value, with the measured displacement at point 4 along the X-axis being ± 0.098 .

Case 2: Arrangement of phase deviation test volume (position 00 - 900; 00 - 1800)

When changing the initial test load mounting position, the position at this time is 00 - 900; 00 - 1800 (i.e. phase angle adjustment), the resulting unbalance parameters are presented below [100].

Table 4.3 Experimental results when mounting the mtrial test load at 00 - 00; $0^0 - 900$, 00 - 1800

No	Location Place <i>the mtrial</i>	Trial Mass (g)	Speed (rpm)	$G = e_p.\omega$ (mm/s)
1	$0^0 - 0^0$		2000	20.5
2	$0^0 - 90^0$	10	2000	14.3
3	$0^0 - 180^0$		2000	2.6
4	$0^0 - 0^0$		2000	32.8
5	$0^0 - 90^0$	20	2000	28.7
6	$0^0 - 180^0$		2000	3.7
7	$0^0 - 0^0$		2000	41.1
8	$0^0 - 90^0$	30	2000	35.4
9	$0^0 - 180^0$		2000	4.2

Correspondingly, we have the results of the displacement measurement at this time:

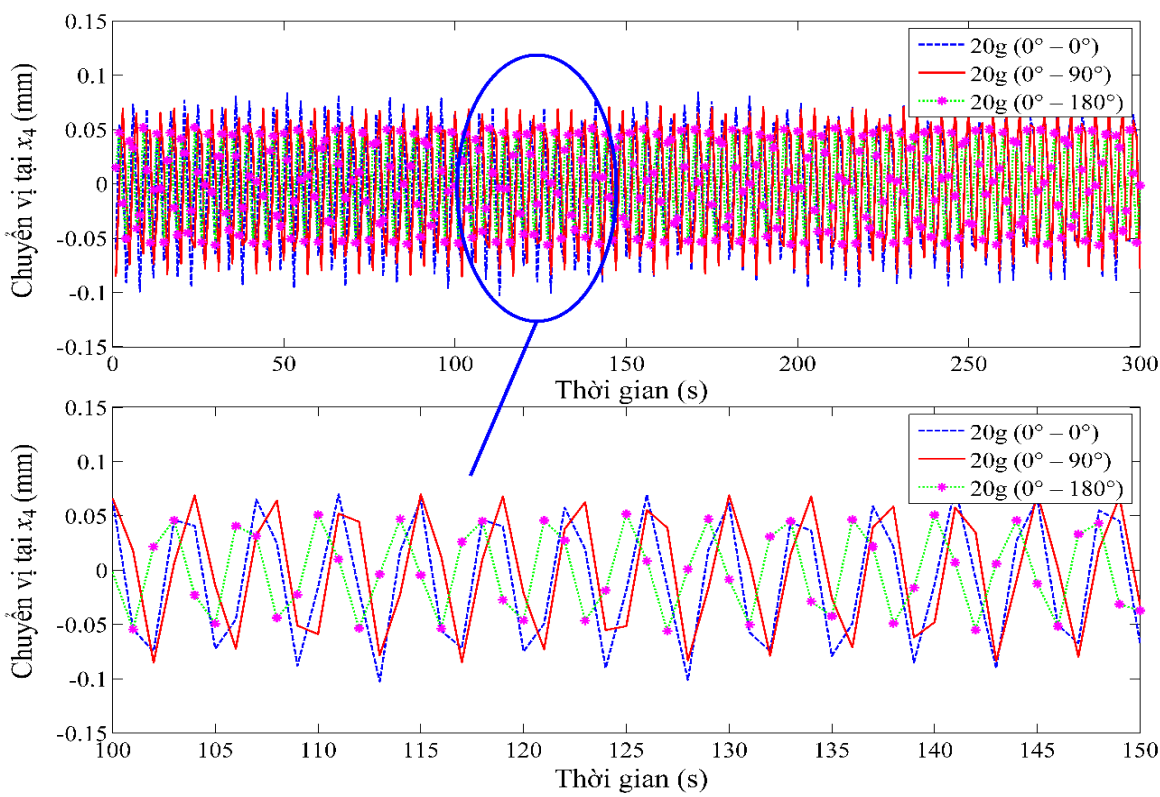


Figure 4.6 The displacement value measured at button 4 with mtrial=20g; n = 2000 rpm, position $0^0 - 00$, 00 - 900; 00 - 1800

Observe:

The measured results (shown in Figure 4.9 and table 4.5) show a decreasing trend in the amount of unbalance and displacement of the axis. Specifically, the experiment at the rotation speed of 2000 rpm with a test load of 20g shows that the adjustment of the load position according to the phase angles from $0^{\circ} - 0^{\circ}$, to $0^{\circ} - 90^{\circ}$, and then to $0^{\circ} - 180^{\circ}$ has caused corresponding changes in the degree of unbalance and displacement value of the rotor:

- In terms of the degree of unbalance, the lowest value achieved at the $0^{\circ} 180^{\circ}$ position is G = 3.7 mm/s, which is fully consistent with the theoretical predictions presented earlier.
- In terms of displacement, the smallest values recorded in the X-axis direction at the load positions $0^{\circ} 0^{\circ}$, $0^{\circ} 0^{\circ}$, and $0^{\circ} 180^{\circ}$, respectively, are \pm 0.098, \pm 0.079; and \pm 0.054, indicating a decreasing trend when the phase angle changes.

3.2.3 Motion trajectory

Figure 4.7 illustrates the trajectory of the rotor at $n_3 = 2000$ rpm under two conditions: when the rotor is not carrying a load and when it is mounted with a 30g load at the $0^{\circ} - 0^{\circ}$ position.

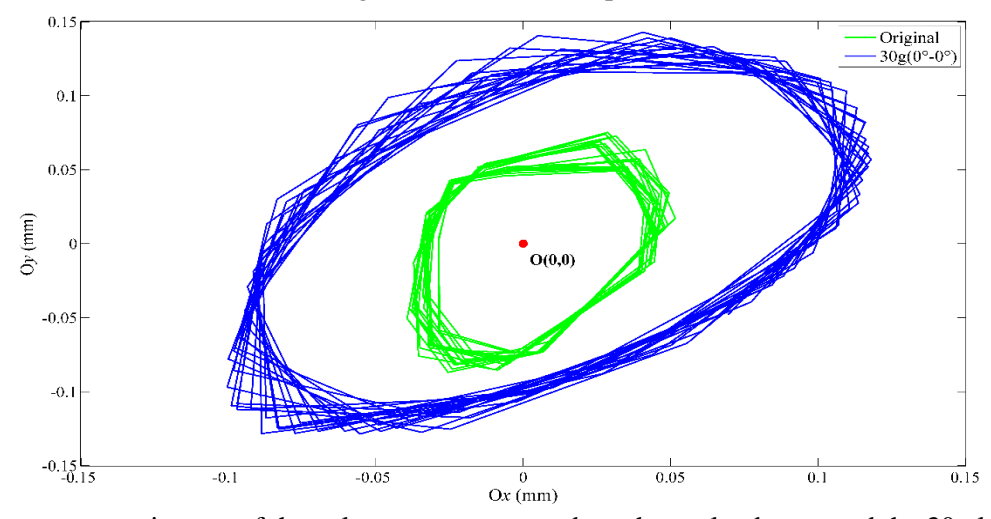


Figure 4.7 The movement trajectory of the axle center corresponds to the no-load rotor and the 30g loaded rotor, Position 0° - 0° ($n_3 = 2000$ rpm)

Table 4.6 Results of displacement measurement at X axis and Y axis in 2 cases: no-load rotor and 30g loaded rotor $(n_3 = 2000 \text{ rpm})$

Speed	No l	load	mtrial = 30 grams		
(rpm)	X (mm)	Y (mm)	X (mm)	Y (mm)	
2000	± 0.046	± 0.081	± 0.109	± 0.135	

Comments:

The experimental data presented in Table 4.6 prove that the trajectory of the rotor clearly reflects the dominance of the predicted regular influence parameters. Moreover, the observation results also show that the amplitude of oscillation with a load mass of 30g, position 0° - 0° , speed of 2000 rpm is greater than the amplitude of oscillation of the rotor at critical speed 1: the largest oscillation recommended to be investigated in experiments. At the same time; the unbalance also reaches the level of G41.3, this amount of unbalance must be avoided during the operation of the rotor to ensure safety and long-term stable operation.

Chapter 5. RESULTS OF CALCULATION AND EXPERIMENT TO EVALUATE FATIGUE RESISTANCE

1. Fatigue curve math model for axial details

Basquin Model

In order to establish the relationship between the stress amplitude and the corresponding number of destruction cycles, Basquin developed a characteristic mathematical model [101]:

$$\sigma_a = \sigma_f'(2N_f)^b \tag{5.1}$$

In which

 σ_a : stress amplitude σ_f' : fatigue strength coefficient

 $2N_f$: number of destruction cycles

b : exponential coefficient Basquin fatigue resistance (b = -0.05 - 0.12)

Remarks: a, b: the experimental constant reflects the structural characteristics of the material and the actual working conditions of the Fatigue detail. Within the framework of the Basquin model, the two main quantities are the stress amplitude σa and the number of cycles $2N_f$. The coefficients σf and b depend on the material properties as well as the geometric shape of the test specimen. Accurate determination of these coefficients requires conducting field testing and processing the corresponding data to derive the necessary values.

The test specimens are rotating parts, which are placed under working conditions with cyclically oscillating stresses. During the load-bearing process, the bearing positions inside the part can form micro-cracks, and when these cracks develop to a certain limit, they will cause damage to the part. On the basis of this phenomenon, the study was conducted to analyze the combined effect of bending, torsion, and unbalance on the rotating part during the fatigue strength evaluation process.

In order to analyze the fatigue strength of the proposed cylindrical detail (see Figure 3.8), the proposed survey point is the weakest point on the model: point 4 corresponds to the horizontal cross section d = 6mm; we have the stress caused by Mu is:

$$\sigma_{max} = \sigma_u = \frac{M_u}{J_x} y_{max} = \frac{M_u}{\frac{J_x}{y_{max}}} = \frac{M_u}{W_u} = \frac{32.F.l}{\pi d^3}$$
 (5.2)

So; the largest stress in this diagram will be the horizontal stress (along the X-axis); corresponding to the force F at this time:

$$F = F_u + F_m = mr\omega^2 + F_m \tag{5.3}$$

In which:

- F_u : Centrifugal force caused by unbalance caused by load mounting;
- F_m : External excitation force / cyclic action (caused by Electromagnet)
- m: test volume;
- r: mounting radius of the test volume;
- ω : angular velocity;

2. Principle diagram and fatigue strength measuring device

At this time; The proposed machine principle diagram is complete as shown in Figure 4.4

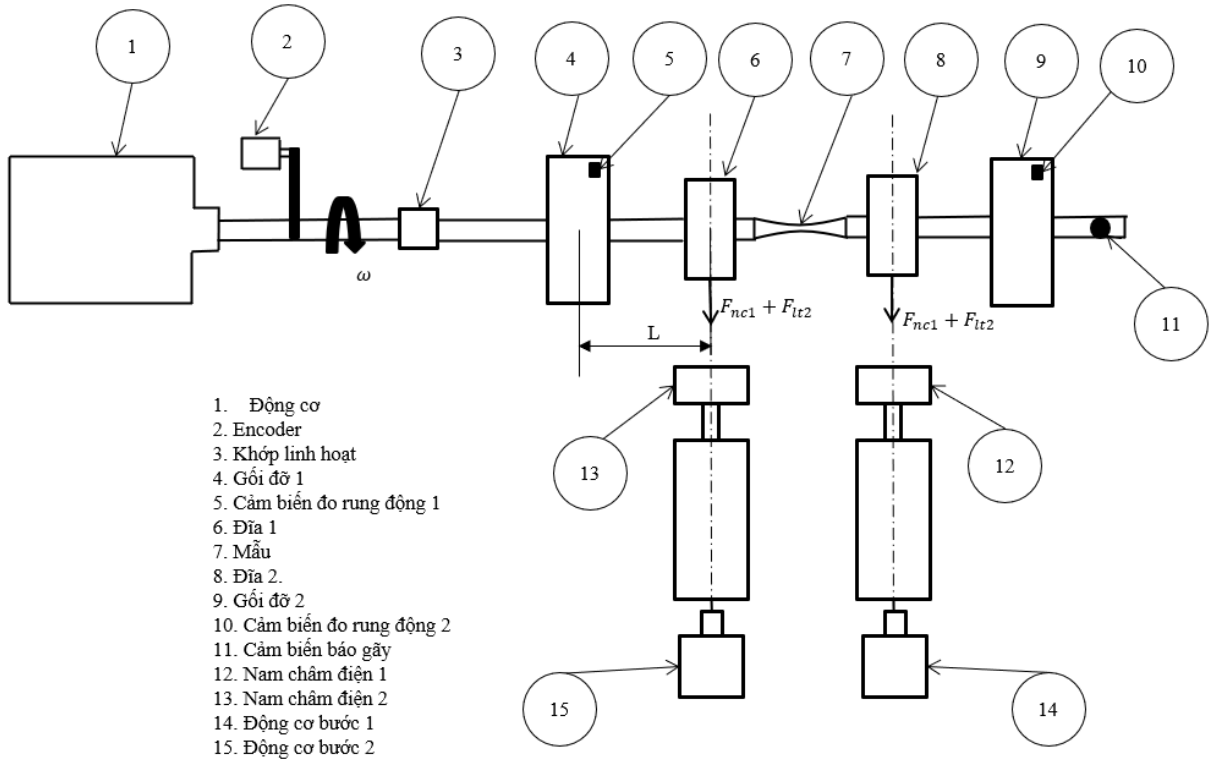
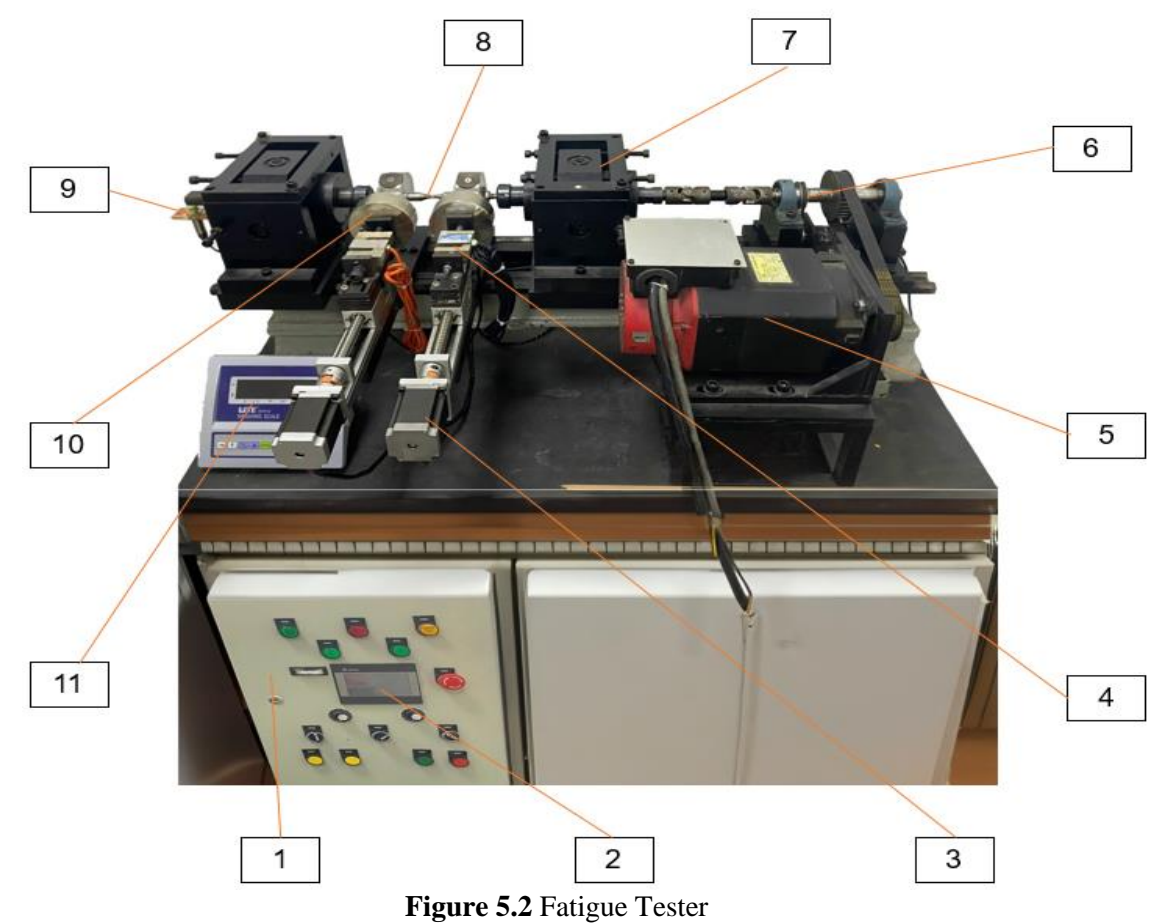


Figure 5.1 Diagram of the applied force using the electromagnet principle

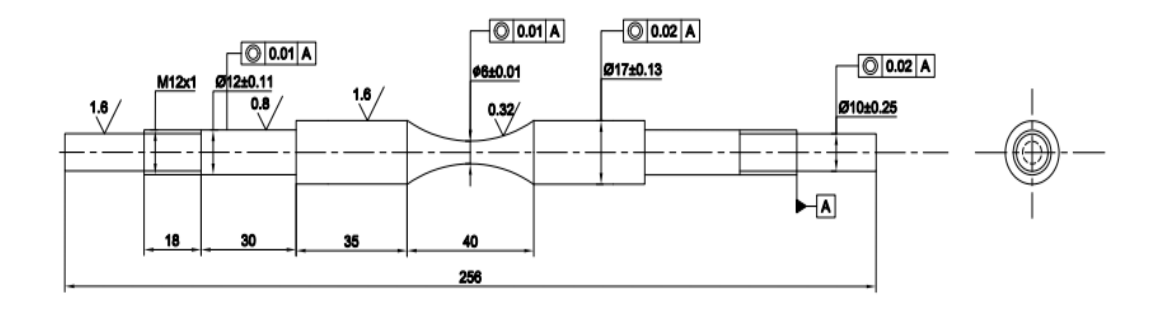
The rotational motion is transmitted by the motor to the active shaft assembly and the passive shaft through a soft coupling system combined with the sample shaft. The fatigue force is applied horizontally to the two discs mounted on the spindle. The magnitude of this force, generated by the electromagnet, will be measured through a load cell. The number of cycles occurs until the part is destroyed due to fatigue is recorded by the Encoder. The factors related to the impact force and the number of operating cycles will be displayed directly on the HMI interface.

The machine after complete fabrication is shown as figure 5.2 including:



18

3. Experiment and evaluation of results Designing Specimens for Fatigue Experiments



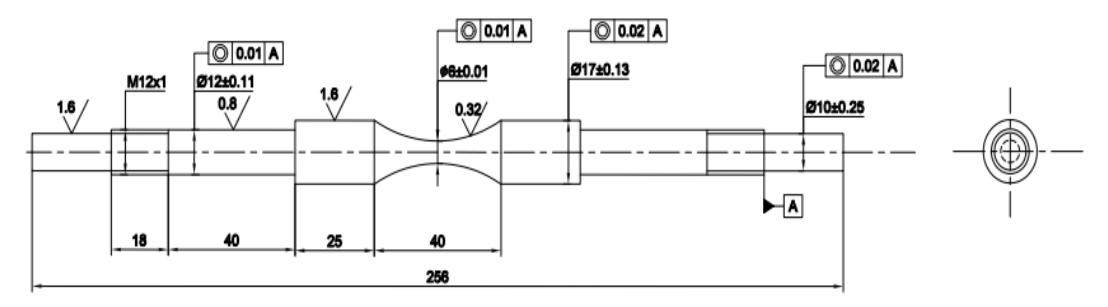


Figure 5.3 Fatigue specimen design ensures compliance with the technical requirements in ISO 1143:2010



Figure 5.4 Experimental samples

Heat Treatment Process

Referring to [70], a new heat treatment procedure is proposed as follows:

Normalized 920°C, 15 minutes, Static Air \rightarrow Normalized 840°C, 15 minutes, Static Air \rightarrow Normalized 760°C, 15 minutes, Static Air.

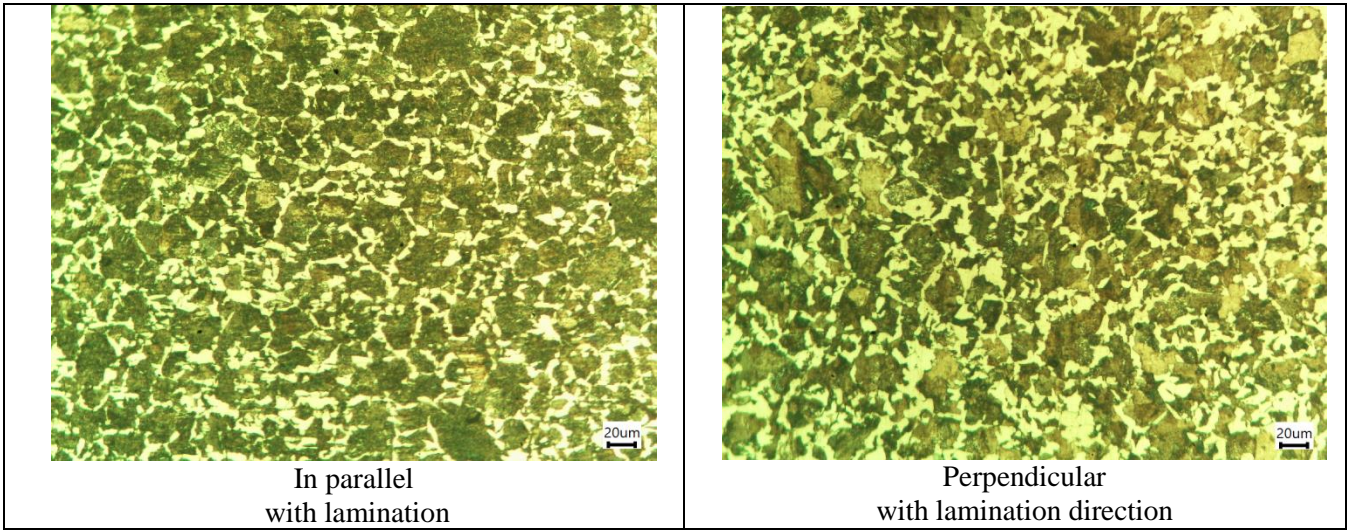


Figure 5.5 Microstructure of C45 steel in the supply state

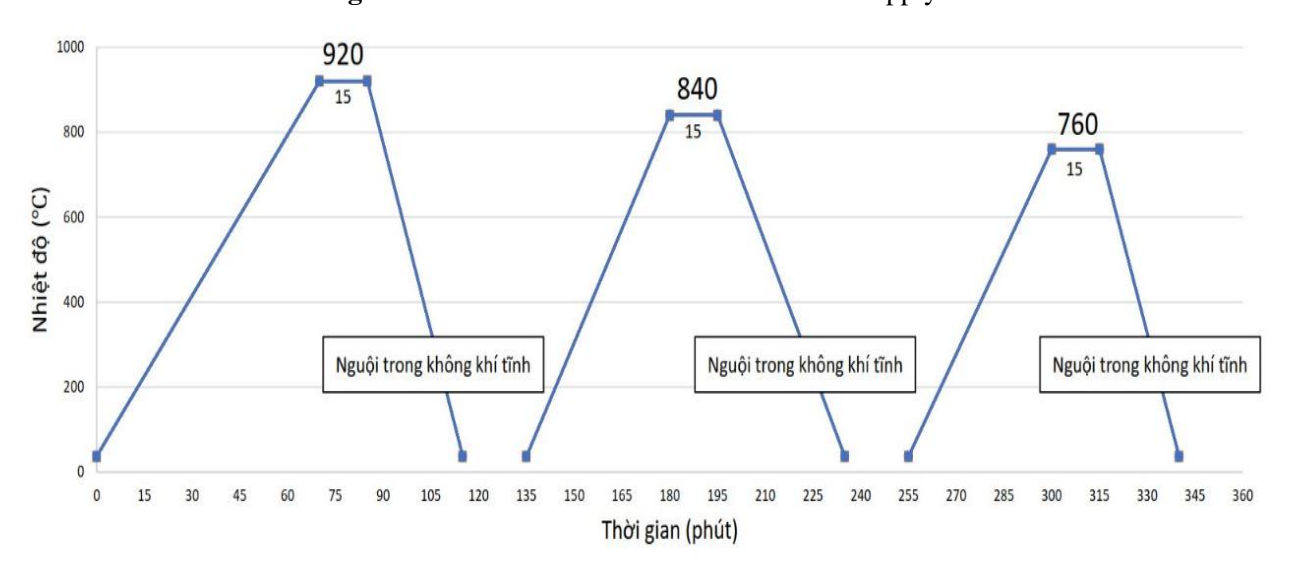


Figure 5.6 Particle shrinking heat treatment process for C45 steel

The parallel with lamination Perpendicular with lamination direction

Figure 5.7 Microstructure of C45 steel after heat treatment

Test the tensile strength of the test specimen

Table 5.1 Tensile test results for C45 steel samples

Sample	Flow Limit σc (MPa)	Endurance limit σb (MPa)	Elongation Relative (%)
1	441	705	21.8
2	412	700	24.2
3	425	713	25
Average	426	706	23,6

Based on the results of Table 4.2; the maximum stress applied in the selected fatigue experiment is equal to 70% of the σ c flow limit, which is equivalent to about 300 MPa. This option ensures that the working stress of the shaft element is within the elastic zone of C45 steel, satisfying the actual operating conditions.

Evaluation of roughness and surface hardness

Table 5.2 Measurement results of Ra sample surface roughness (μm)

Experimental Sample	1	2	3	Average
Roughness (μm)	0,325	0,328	0,324	0,32

Table 5.3 Test results of test specimen surface hardness

Test Specimen	1	2	3	Average
Hardness (HRB)	86	87	86.5	86.5

4.4 Experimental results

From the data collected (shown in Table 4.6), the fatigue curve was constructed based on Basquin's equation, with the support of calculation and data processing using Excel software. From equations (4.5) and (4.6) we make Table 4.5 showing the relationship between the parameters affecting the unbalance on the axis of rotation and stress. Since σ max = 70% σ c \approx 300 Mpa, we select the test points with the corresponding stresses; according to Table 4.2 we have an unbalance at 1500 rpm of G = 14.3.

Table 5.4 Conversion from Parameters Affected by Stress Unbalance

STT	Load m (g)	Radius Load R (mm)	Speed (rpm)	Centrifugal force F _u (N)	Magnet Force F_m (N)	Stress σ (MPa)
Point 1	30	50	1200	23,7	10	286
Point 2	30	50	1100	19,9	10	254
Point 3	30	50	1010	16,8	10	228
Point 4	30	50	900	13,3	10	198
Point 5	30	50	870	12,4	10	190

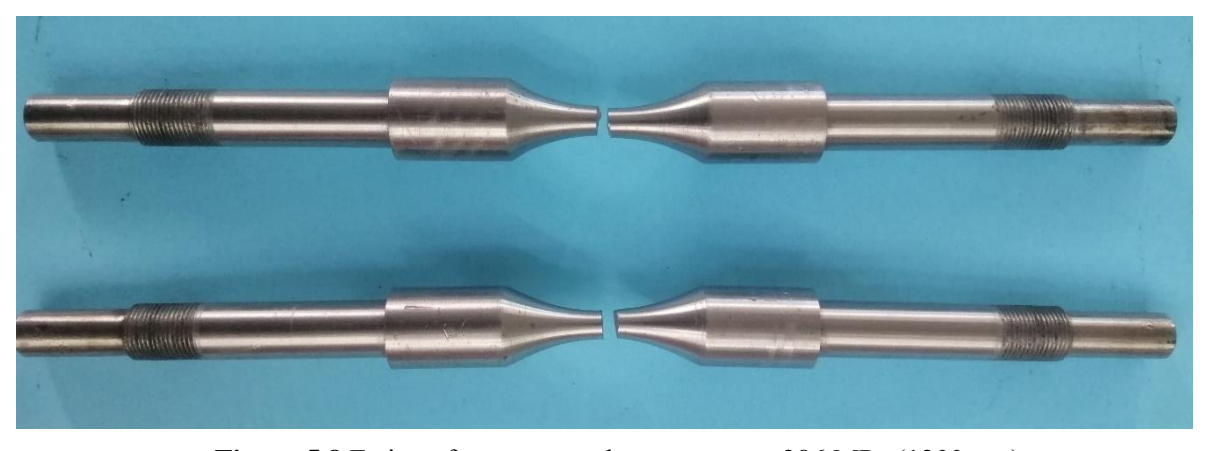


Figure 5.8 Fatigue fracture sample at stress $\sigma = 286$ MPa (1200rpm)

Table 5.5 Summary of data obtained from the experiment

Material	Sample	Stress Level 1 $\sigma = 286$ (MPa)	Stress Level 2 σ =254 (MPa)	Stress Level 3 $\sigma = 228$ (MPa)	Stress Level 4 σ =198 (MPa)	Stress level 5 $\sigma = 190$ (MPa)
		Number of cycles	Number of cycles	Number of cycles	Number of cycles	Number of cycles
Steel C45	1	241.460	651.000	3.913.200	6.885.000	10.000.000
	2	263.140	715.100	3.151.000	5.540.000	10.000.000
	3	229.670	611.000	3.510.000	4.800.000	10.000.000

Based on the data collected from the experiment, the fatigue curve of the C45 steel material was established with the help of Excel software. Figure 4.17 illustrates the fatigue curve corresponding to the spindle pattern detail.

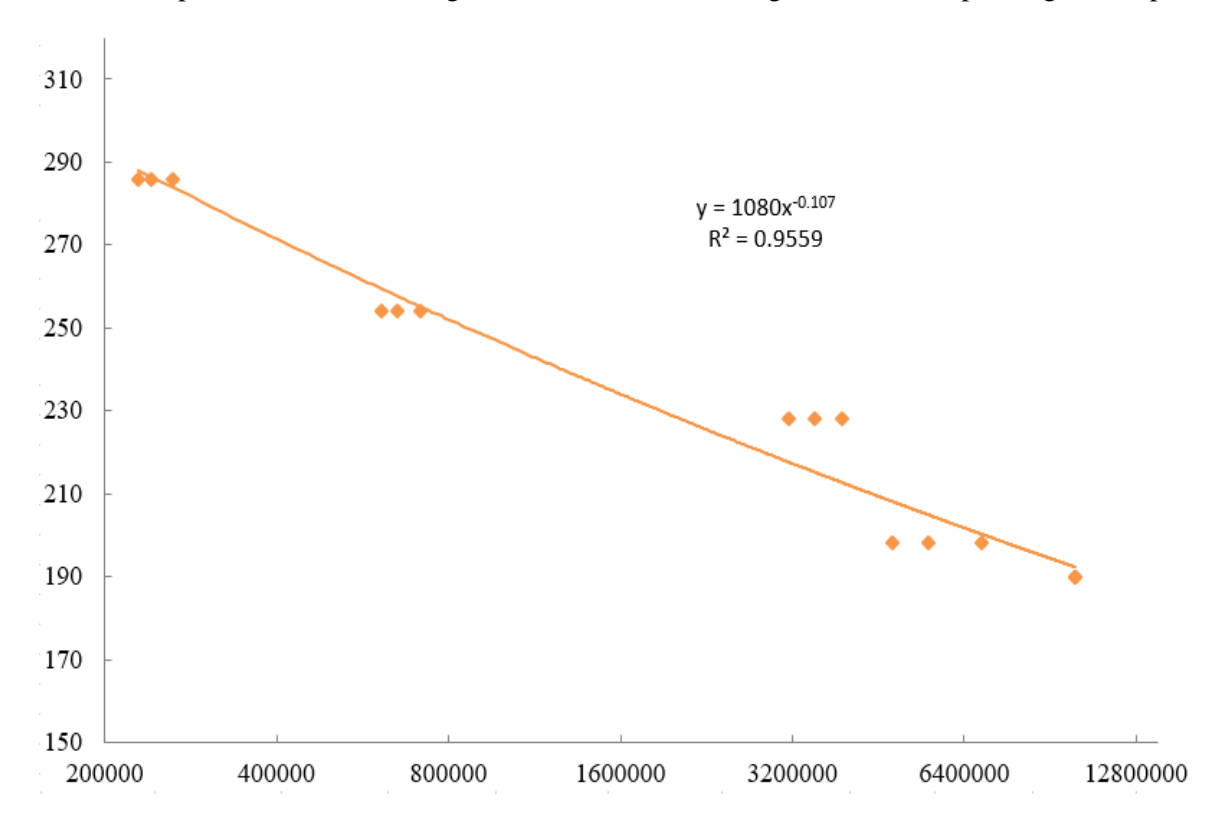


Figure 5.9 Experimental fatigue curve corresponding to C45 steel material

The equation representing the stress-cycle relationship according to the Basquin model for C45 steel is established from the following experimental data:

$$\sigma_a = 1080.(2N_f)^{-0.107}$$

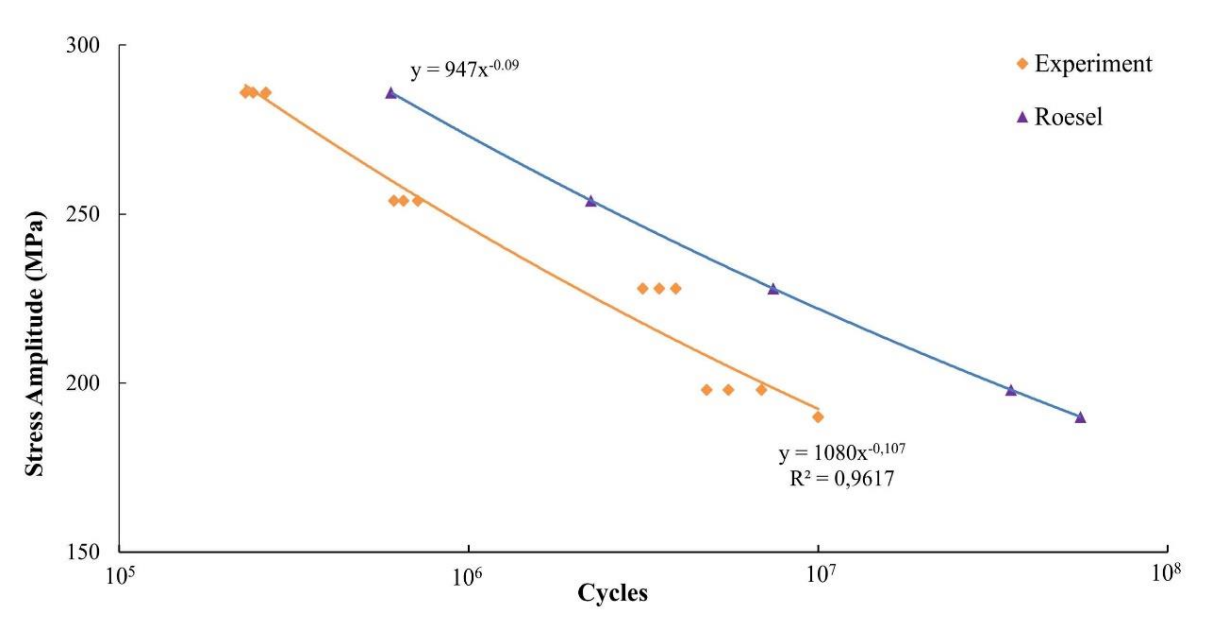


Figure 5.10 Experimental fatigue curve from C45 steel against the Roesel curve

Observe:

This can be explained by the fact that, as the applied stress increases, the propagation rate of cracks in the material also increases, leading to the phenomenon of part destruction occurring earlier.

Compared to the fatigue curve of Roesel experimented with pure bending, the results show that the parameters affect the unbalance on the axis of rotation resulting in a decrease in fatigue strength compared to the pure bending sample.

Chapter 6. CONCLUSION AND DEVELOPMENT DIRECTION

Results achieved

In this thesis, the author has focused on studying the influence of unbalance factors on the fatigue strength of the rotor, namely the spindle. The parameters surveyed include: rotation speed, test mass (causing unbalance), initial phase angle and external force. Build a mathematical model and apply the Newmark numerical method $-\beta$ to solve the above problem. Design and manufacture of 2 instruments for experimental purposes: oscillation meter and fatigue tester. These devices play an important role in validating theoretical models and providing empirical data for analysis. Establish the relationship between stress and cycle (S-N): the fatigue curve shows the relationship between factors that affect the unbalance to fatigue endurance. The results of the study contribute to clarifying the mechanism of the influence of unbalance factors on the working state of the rotor, thereby providing a basis for the design, balancing and diagnosis of damage in industrial rotating mechanisms. The main research results achieved are as follows:

- Determine the parameters that directly affect the dynamic unbalance in the axis of rotation: rotation speed, eccentric mass and position of the unbalance mass.
- The vibration becomes unstable when the rotation speed reaches the critical speed and the displacement amplitude increases significantly. At the same time, the amount of unbalance increases (to G40) resulting in an increase in the displacement amplitude. The amplitude of the fluctuation in the case of G41.3 has $X = \pm$ 0.109; $Y = \pm$ 0.135 is even greater than the amplitude of fluctuation at critical speed 1: $X = \pm$ 0.101; $Y = \pm$ 0.119. This is the amplitude of fluctuation to be avoided during operation to ensure stable and long-term operation of the rotor.
- The initial phase angle of the test mass position, if a change occurs during operation, will result in different variations of the vibration phase causing the bending stress to increase or decrease which may result in failure appearing on the spindle.
- The results of this study also demonstrate that the Newmark-β method used to analyze the behavior of the rotor system has high reliability, unconditional stability, fast convergence time and high accuracy, with an error of < 6% compared to the experiment.
- A new testing machine for studying the fatigue endurance of unbalanced drive shafts has been developed. A new control program alignment tool is also designed to assess these disproportionate effects.
- The results of the fatigue strength test showed that the fatigue limit and fatigue strength of the sample decreased under the influence of unbalanced factors; including test volume, operating speed and load radius; compared to the pure bending spindle, thereby successfully constructing the stress-cycle curve for the C45 steel spindle part under the action of forces that cause unbalance.

- In addition, the amplitude of oscillation will become larger and larger as the load cycle increases. This can be explained by the appearance and propagation of microcracks, amplifying the effect of unbalanced forces on the spindle.

Development direction

In addition to the results achieved and the scope of research of the project, the research direction of the project also has many fields that can be exploited:

- Applying the above model in the development of Online *Codition Monitoring (OCM)*, *Vibration Condition Monitoring (VCM)* or *Structural Health Monitoring (SHM)* or combining systems together to help predict the remaining lifespan. optimize dynamic balance, and ensure long-term operational safety.
- Further research is needed to understand the impact of different parameters on the fatigue life of the spindle under different operating conditions such as high temperature, high speed (especially critical speed 2) or in terms of materials: multiphase materials, 42CrM04, stainless steel (SUS 304; 316; 420); aluminum alloy (6061, 7075) or composite material.
- In addition, we will apply scanning electron microscopy (SEM) techniques to evaluate fatigue cracks in subsequent studies.

Published works

- 1. Lam T.T, Ngon D.T, Cuong L.C; Study on the Applicability of Influence Coefficient Method Combined with Vector Analysis in Dynamic Balancing Rigid Rotor Using Flexible Supports; Proceedings 2018 4th International Conference on Green Technology and Sustainable Development, pp. 228-231, 2018.
- 2. Tran Thanh Lam; Research, manufacture and experiment of soft shaft rotor model; Journal of Science and Technology No. 58, 2020.
- 3. Tran Thanh Lam, Dang Thien Ngon, Tran Thai Son, Le Chi Cuong; Experimental study to evaluate the parameters that affect the oscillation of the rotor; Journal of Science and Technology, No. 66/2021.
- 4. Lam T.T, Cuong C.L et al; *An experimental study evaluating parameters effects on the vibration of rotor;* AIP Conference Proceedings 2420, 070003, 2021.
- 5. Thanh Lam Tran, Vinh Phoi Nguyen, Chi Cuong Le, Thien Ngon Dang; *Effect of unbalanced parameters on the fatigue behavior of transmission shaft in gearbox*; Strength, Fracture and Complexity, 18(2), pp.86-92, 2025 (ISI-Q4).
- 6. Thanh Lam Tran, Vinh Phoi Nguyen, Chi Cuong Le, Thien Ngon Dang; *Investigation on the Influence of Unbalanced Shaft Component in Gearbox on Displacement Using the Newmark-β Method;* PLOS ONE (SCIE Q1), revised following the second round of review.